Supporting Information

Photo- and thermo-responsive microgels with supramolecular crosslinks for wavelength tunability of the volume phase transition temperature

Wenjing Liang,[a] Carlos G. Lopez,[a] Walter Richtering,[a] and Dominik Wöll*[a]

[a] *Institute of Physical Chemistry, RWTH Aachen University, Landoltweg 2, 52074 Aachen, Germany.*
Tel: +49 241 80 98624; E-mail: woell@pc.rwth-aachen.de

Contents

1 Synthesis

1.1 Synthesis of mono-β-cyclodextrin acrylamide (βCD-AA)

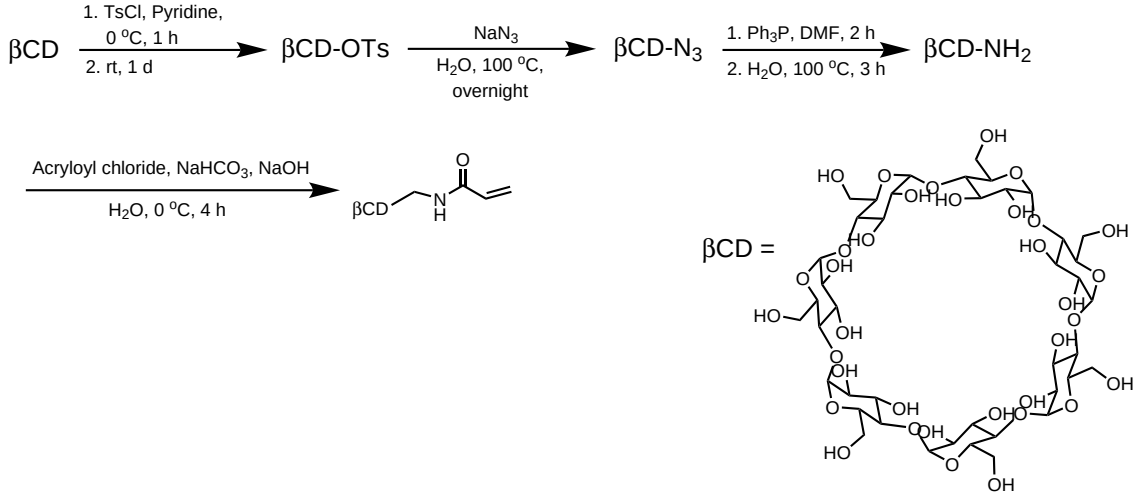

Figure S1 Synthesis of **βCD-AA**

The mono-β-cyclodextrin acrylamide **βCD-AA** was synthesized according to literature.[1] ^{1}H – NMR (600 MHz, D_2O, 298 K) δ (ppm): 6.28 (d, J = 17.4 Hz, 1H), 6.03 (dd, J = 17.4 Hz, 10.8 Hz, 1H), 5.89 (d, J = 10.8 Hz, 1H), 4.91 (m, 7H), 3.88-3.90 (m, 7H), 3.68–3.78 (m, 28H), 3.49–3.78 (m, 7H), 3.45 (t, J = 9.6 Hz, 14H).

1.2 Synthesis of mono-PEG-Azo acrylamide (Azo-AA)

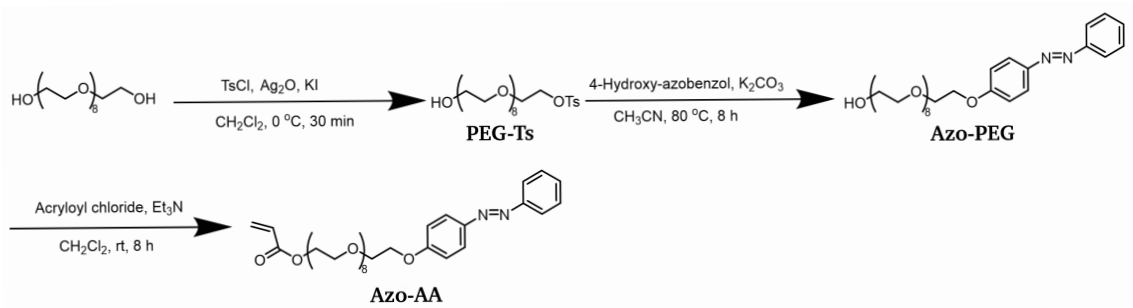

Figure S2 Synthesis of **Azo-AA**.

For monotosylation,[2] p-toluenesulfonyl chloride (TsCl, 1000 mg, 5.25 mmol), potassium iodide (KI, 175 mg, 1.05 mmol), and fresh silver oxide (Ag_2O, 1825 mg, 7.88 mmol) was added to a solution of poly(ethylene glycol) (PEG400, $M_w \approx 400$ g/mol, 2100 mg, 5.25 mmol) in dry dichloromethane cooled to 0 °C in a water bath. After addition, the mixture was stirred at 0 °C for 1 h. Subsequently, silver oxide was removed by filtration. After the solvent had been removed under reduced pressure, the residue was extracted with DCM (3 × 50 mL) and washed with brine (50 mL), water (50 mL), then the organic layer was dried over Na_2SO_4 and concentrated *in vacuo*. The crude product was purified by column chromatography (SiO_2, DCM:MeOH = 50:1) to afford **PEG-Ts** as a colorless oil (1000 mg, yield 75%). ^{1}H – NMR (600 MHz, $CDCl_3$, 298 K) δ (ppm): 7.78 (d, J = 12.6 Hz, 2H), 7.33 (d, J = 12.0 Hz, 2H), 4.14 (t, J = 7.2 Hz, 2H), 3.57–3.70 (m, 30 H).

To a solution of **PEG-Ts** (500 mg, 0.9 mmol) in MeCN was added 4-hydroxyazobenzene (163 mg, 0.82 mmol). Subsequently, potassium carbonate (170 mg, 1.23 mmol) was added, and the mixture was stirred at 80 °C under argon atmosphere for 8 h. After removing the solvent under reduced pressure, the residue was extracted with DCM (3 × 50 mL) and washed with brine (50 mL), water (50 mL), then the organic layer was dried over Na_2SO_4 and concentrated *in vacuo*. The crude product was purified by column chromatography (SiO_2, DCM:MeOH = 30:1) to afford **Azo-PEG** as a yellow oil (400 mg, yield 75%). ^{1}H – NMR (600 MHz, $CDCl_3$, 298K) δ (ppm): 7.89 (d, J = 9.0 Hz, 2H), 7.86 (d, J = 7.8 Hz, 2H), 7.48 (t, J = 7.8 Hz, 2H), 7.42 (m, 1H), 7.01 (d, J = 8.4 Hz, 2H), 4.29 (t, J = 4.8 Hz, 2H), 4.20 (t, J = 4.8 Hz, 2H), 3.88 (t, J = 4.8 Hz, 2H), 3.57–3.78 (m, 25 H). ^{1}3C – NMR (151 MHz, $CDCl_3$, 298 K) δ (ppm): 166.22, 161.34, 152.79, 147.12, 131.08, 130.44, 129.08, 128.34, 124.76, 122.61, 114.90, 70.93, 70.68, 70.66, 70.61, 69.67, 69.15, 67.79, 63.74.

Triethylamine (3.75 mg, 0.04 mmol) was added to a solution of **Azo-PEG** (200 mg, 0.34 mmol) in DCM. Acryloyl chloride (4.19 mg, 0.41 mmol) was added dropwise in an ice bath. After reacting for 12 h, the solvent was removed *in vacuo*. The product was purified by flash chromatography (SiO_2, DCM:MeOH = 30:1) to afford **Azo-AA** as a yellow oil (128 mg, yield 55%). ^{1}H – NMR (600 MHz, $CDCl_3$, 298K) δ (ppm): 7.89 (d, J = 9.0 Hz, 2H), 7.86 (d, J = 7.8 Hz, 2H), 7.48 (t, J = 7.8 Hz, 2H), 7.42 (m, 1H), 7.01 (d, J = 8.4 Hz, 2H), 6.41 (d, J = 17.4 Hz, 1H), 6.14 (dd, J = 17.4 Hz, 10.8 Hz, 1H), 5.82 (d, J = 10.8 Hz, 1H), 4.29 (t, J = 4.8 Hz, 2H), 4.20 (t, J = 4.8 Hz, 2H), 3.88 (t, J = 4.8 Hz, 2H), 3.57–3.78 (m, 25H). ^{1}3C – NMR (151 MHz, $CDCl_3$, 298 K) δ (ppm): 166.22, 161.34, 152.79, 147.12, 131.08, 130.44, 129.08, 128.34, 124.76, 122.61, 114.90, 70.93, 70.68, 70.66, 70.61, 69.67, 69.15, 67.79, 63.74.

1.3 NMR spectra of synthesized compounds

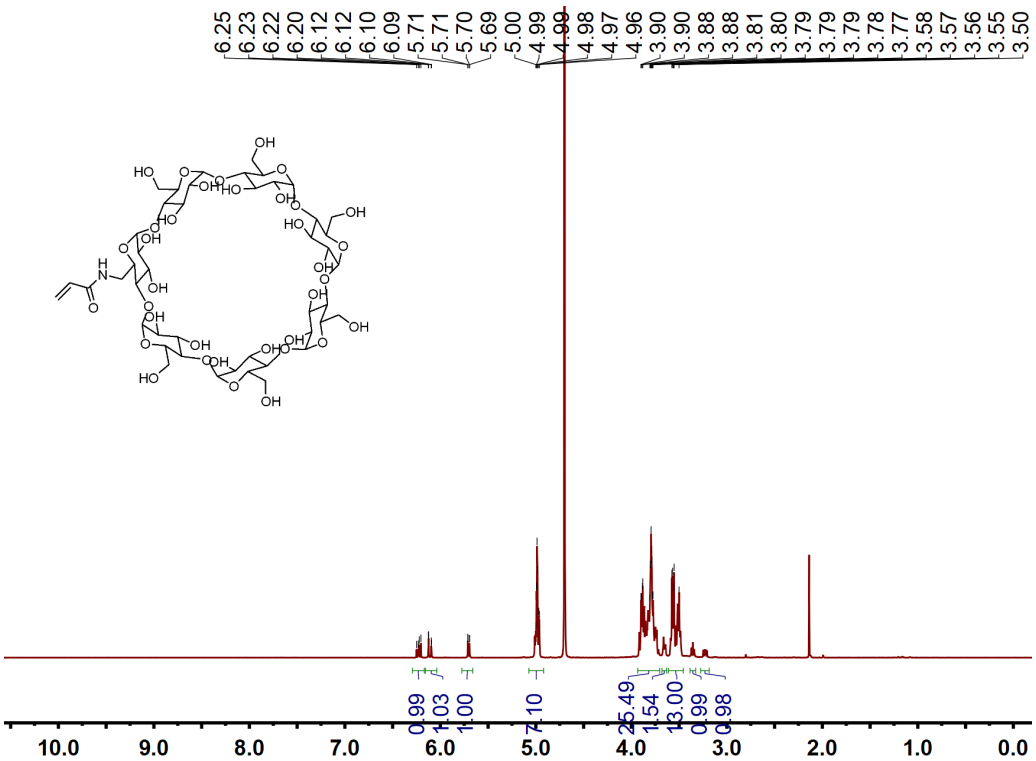

Figure S3 ^{1}H-NMR spectrum of ***β*CD-AA** (600 MHz, D_2O, 298 K)

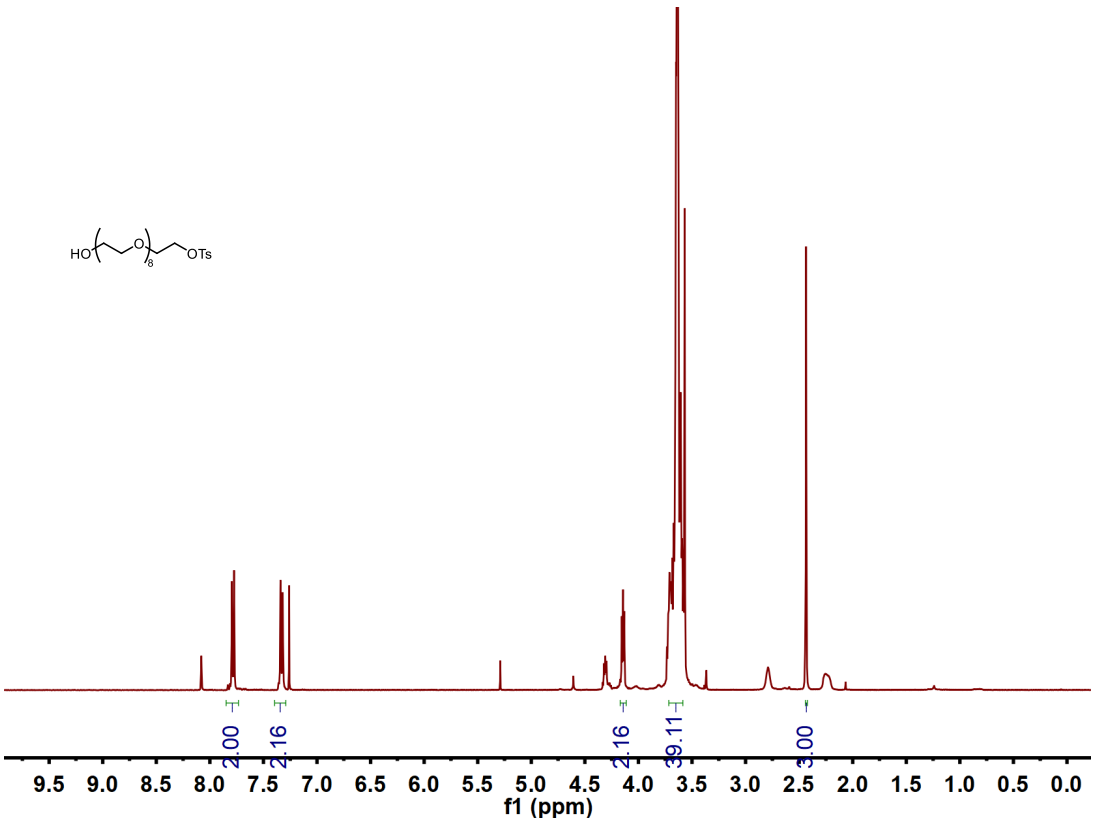

Figure S4 ^{1}H-NMR spectrum of **PEG-Ts** (600 MHz, D_2O, 298 K)

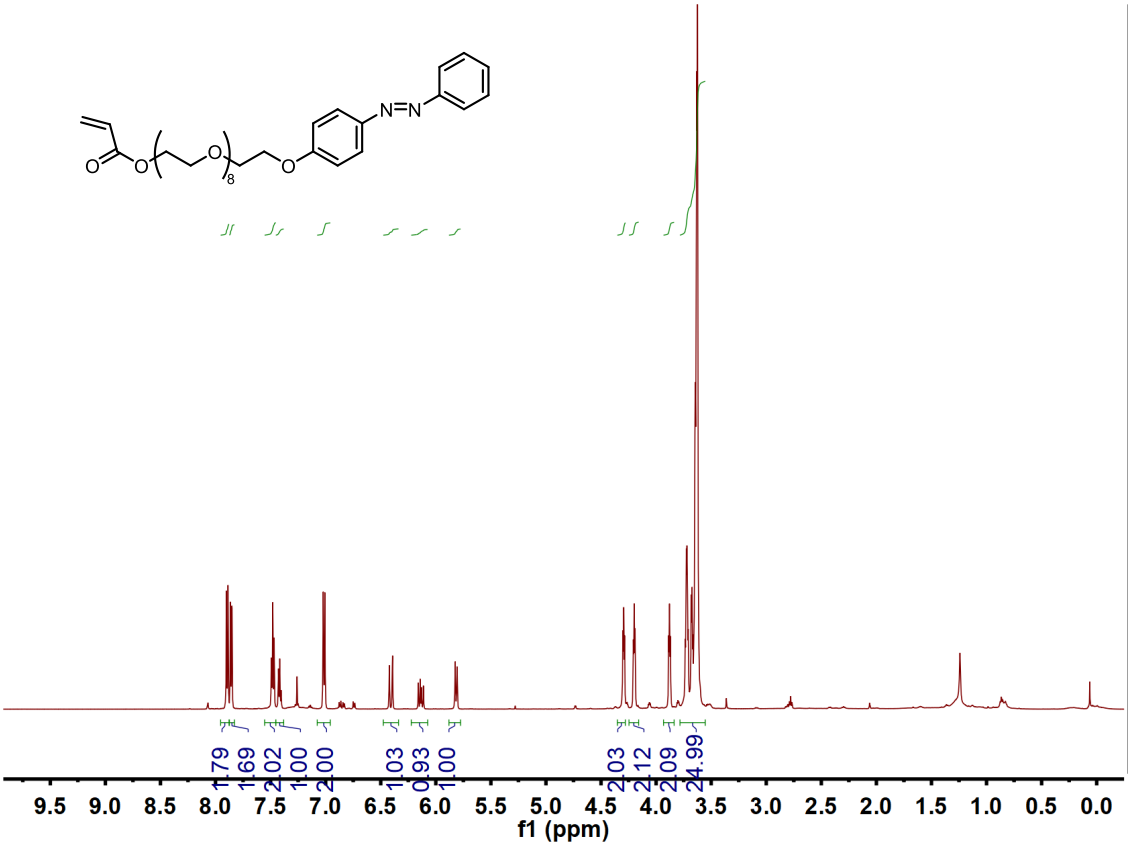

Figure S5 ^{1}H-NMR spectrum of **Azo-PEG** (600 MHz, D_2O, 298 K)

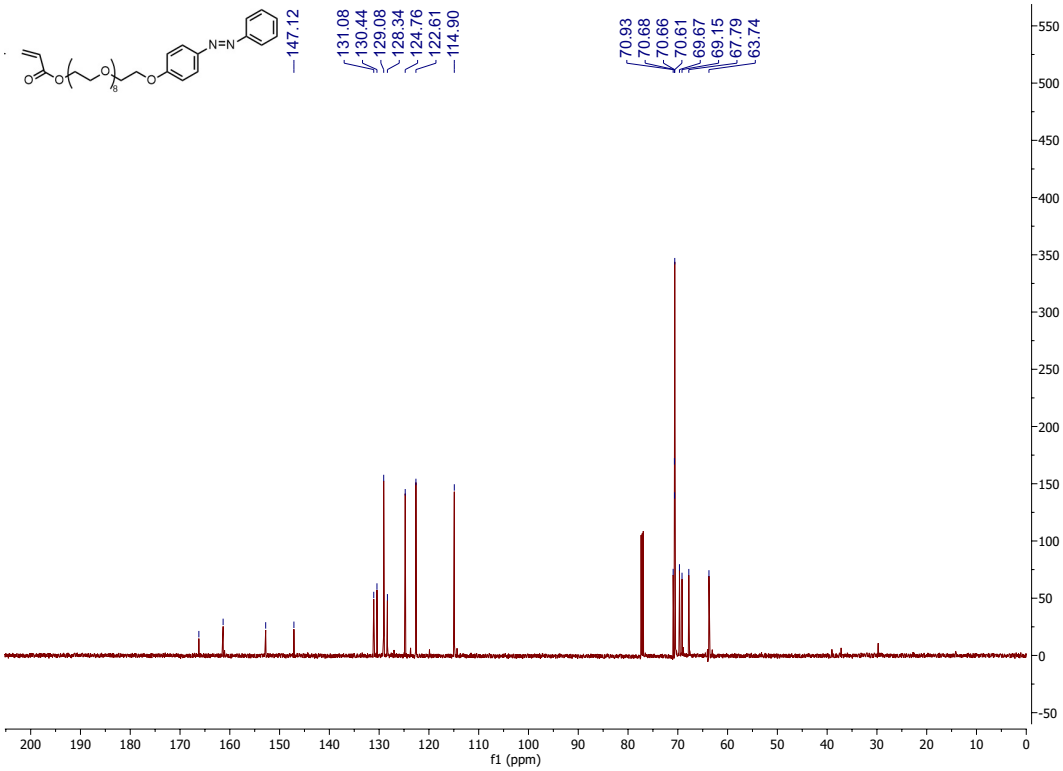

Figure S6 ^{1}H-NMR spectrum of **Azo-AA** (600 MHz, D_2O, 298 K)

1.4 Absorption coefficient of Azo-AA

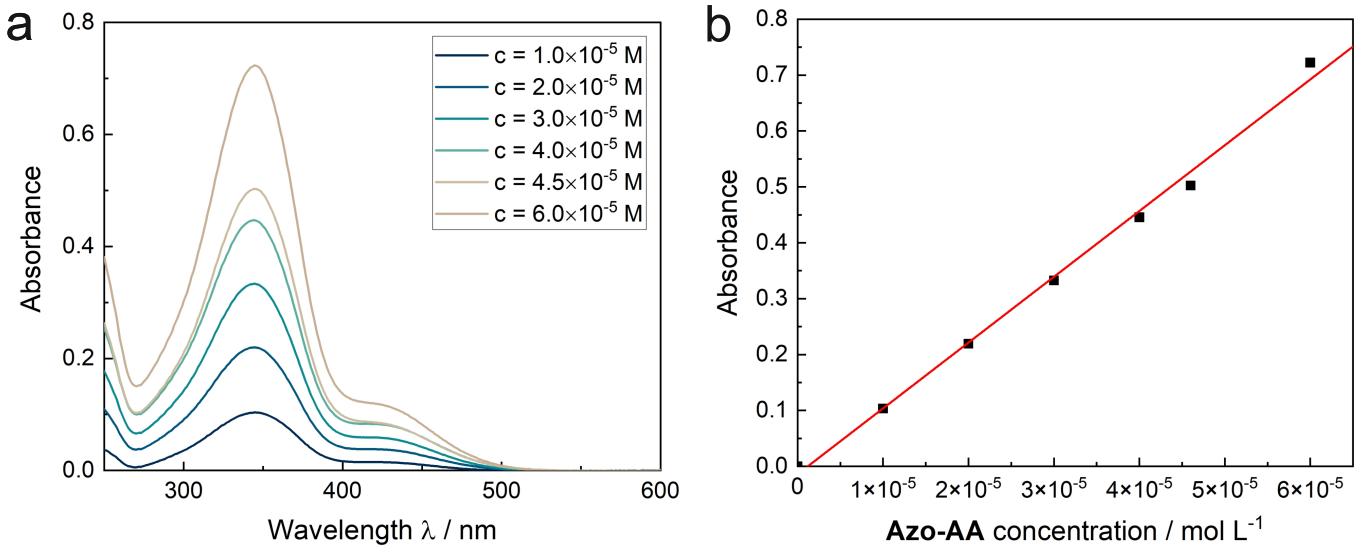

Figure S7 Calibration curve of **Azo-AA** in water at different concentrations. An absorption coefficients of 11769 L mol^{-}1 cm^{-}1 was obtained from the slope of the curve in (b).

2 Photochemical *trans-cis* isomerization of Azo-AA

2.1 Changes of absorption spectra after irradiation

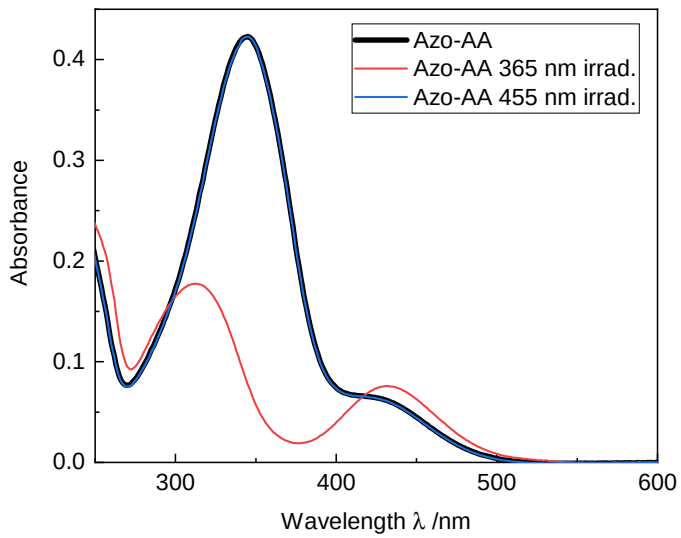

Figure S8 UV-Vis absorption spectra of the monomer **Azo-AA** in its initial form, after UV irradiation (λ_{UV} = 365 nm, light intensity 5.37 W m^{-2}) and after subsequent irradiation with visible light until the photostationary state was reached (λ_{Vis} = 455 nm, light intensity 22.1 W m^{-2}).

2.2 NMR analysis of *trans-cis* isomerization after irradiations

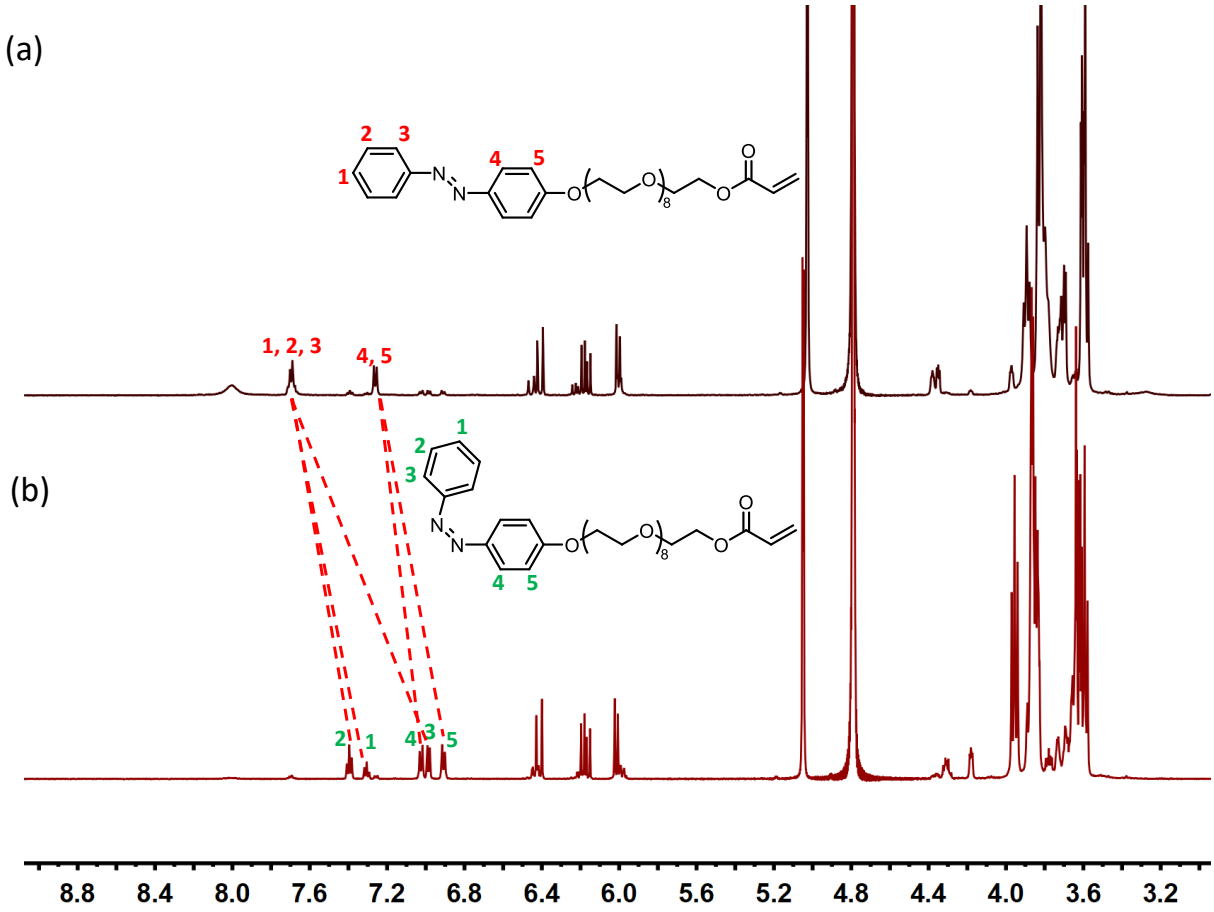

Figure S9 ^{1}H-NMR spectrum (600 MHz, 5 mM, D_2O, 298 K) of the ***β*CD-AA/Azo-AA** complex with 2:1 mix ratio (a) before and (b) after UV irradiation for 15 min (λ_{UV} = 365 nm, light intensity 5.37 W m^{-2}, 600 MHz, D_2O, 298 K).

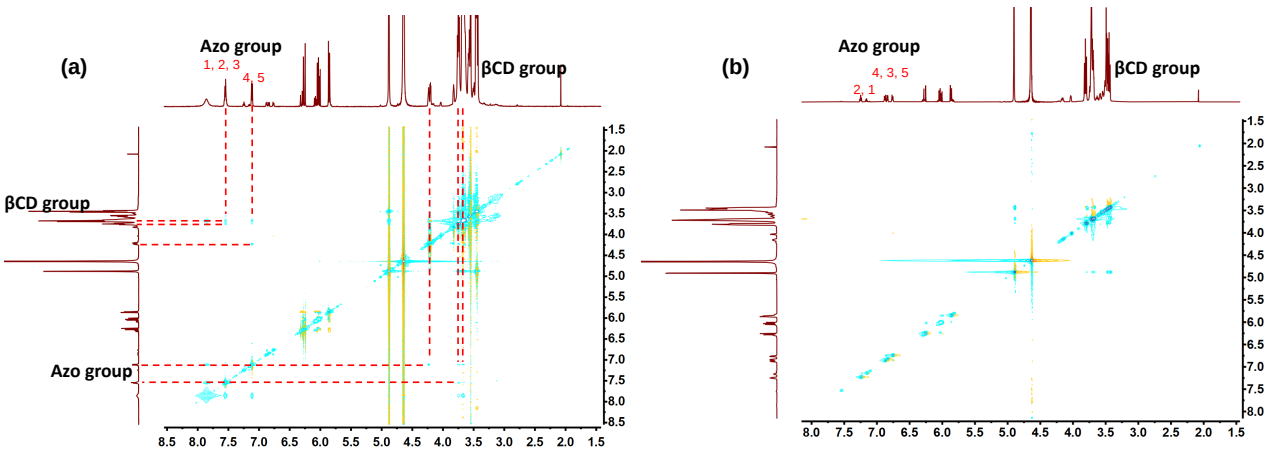

Figure S10 2D-NOESY spectra (600 MHz, 5 mM, D_2O, 298 K) of the ***β*CD-AA/Azo-AA** complex with 2:1 mix ratio: (a) the complex before UV irradiation; (b) ***β*CD-AA** and predominantly the *cis* form of **Azo-AA** after UV irradiation for 15 min (λ_{UV} = 365 nm, light intensity 5.37 W m^{-2}).

2.3 Photokinetics of the Azo-AA and βCD-AA/Azo-AA

The photokinetics of free **Azo-AA**, the complex ***β*CD-AA/Azo-AA** in aqueous solution and the photoresponsive microgels containing the complex as crosslinker were investigated by UV-vis spectroscopy. As can be seen in Figure S11a, the trans ***trans*Azo-AA** shows a characteristic π–π^* absorption peak around 350 nm and a weak n–π^* electronic transition band around 440 nm. Under UV light irradiation (365 nm), the intensity around 350 nm decreased significantly and the peak shifted hysochromically. Simultaneously, the intensity around the 440 nm increased. With the light source used, a photostationary state between ***trans*Azo-AA** and ***cis*Azo-AA** was reached after approx. 15 min. This process follows the first-order kinetics equation:

$$\ln \frac{A_t - A_\infty}{A_0 - A_\infty} = -kt$$

where k is a first order rate constant, and A_0, A_t, and A_∞ are the absorbance values at a specific wavelength before irradiation, after irradiation time t, and in the photostationary state ($t = \infty$), respectively. Figures S11 and S12 show that the photokinetics of free **Azo-AA** is faster than the one of azobenzene in the ***β*CD-AA/Azo-AA** complex.

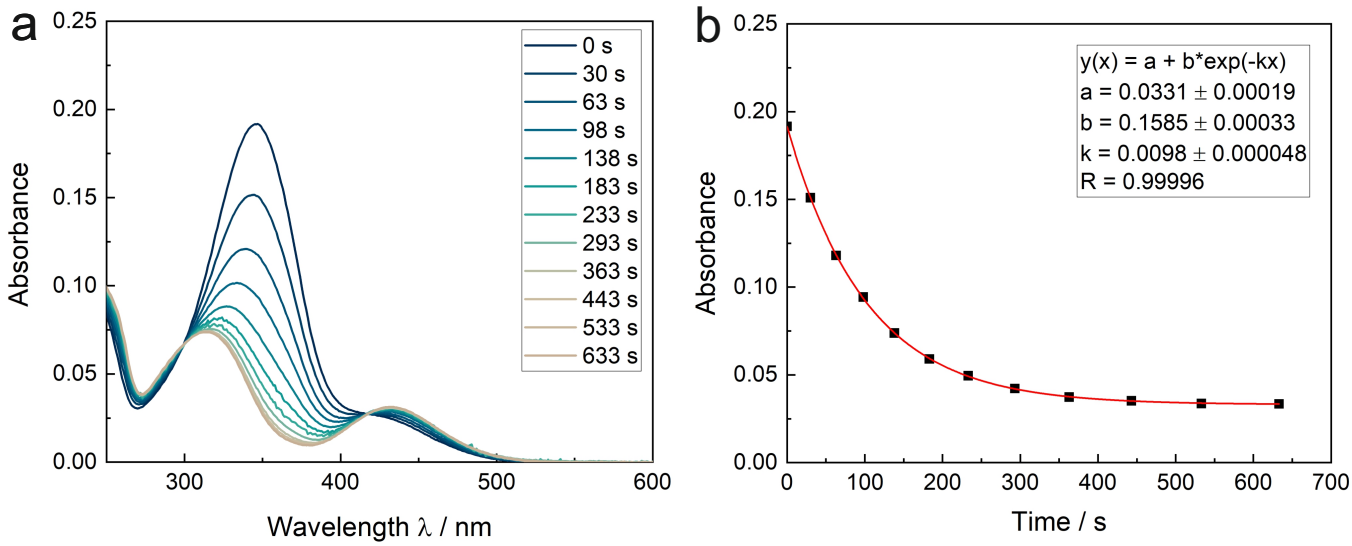

Figure S11 (a) Absorption spectra of free **Azo-AA** reacting from the *trans* to mainly the *cis* isomer until reaching the photostationary state by irradiation with 365 nm (5.38 W/m^2, 0.02 mM in water); (b) Photokinetics of free azobenzene from the *trans* isomer to the photostationary state with mainly the *cis* isomer for the condition as stated in (a). The solid line represents the data fitting according to a first-order equation.

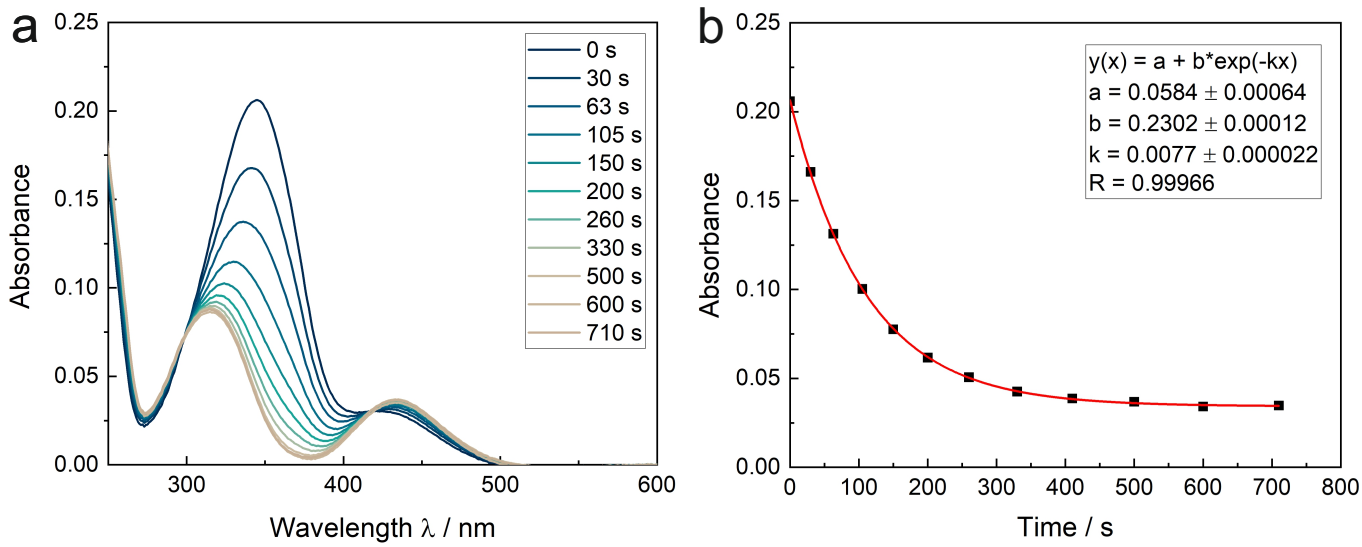

Figure S12 (a) Absorption spectra of **Azo-AA** bound to β-cyclodextrin (**Azo-AA** : **βCD-AA/Azo-AA** = 1 : 40) reacting from the *trans* to mainly the *cis* isomer until reaching the photostationary state by irradiation with 365 nm (5.38 W/m^2, 0.02 mM in water); (b) Photokinetics of **Azo-AA** : **βCD-AA/Azo-AA** = 1 : 40 from the *trans* isomer to the photostationary state with mainly the *cis* isomer for the condition as stated in (a). The solid line represents the data fitting according to a first-order equation.

Table S1 Switching properties of the free azobenzene and the mixture with cyclodextrin in water: rate constants k and quantum yields ϕ for the *trans-cis* and for the *cis-trans* isomerization.

Sample	$k_{t\to c}/10^{-3}$ s^{-1}	$\phi_{t\to c,346\text{ nm}}$	$k_{c\to t}/10^{-3}$ s^{-1}	$\phi_{c\to t,346\text{ nm}}$
Azo-AA	9.82 ± 0.05	0.251 ± 0.001	5.83 ± 0.05	0.052 ± 0.001
Azo-AA : βCD-AA/Azo-AA = 1 : 2	9.53 ± 0.05	0.244 ± 0.001	5.58 ± 0.05	0.039 ± 0.001
Azo-AA : βCD-AA/Azo-AA = 1 : 4	8.98 ± 0.01	0.229 ± 0.001	5.00 ± 0.04	0.041 ± 0.001
Azo-AA : βCD-AA/Azo-AA = 1 : 20	8.18 ± 0.10	0.207 ± 0.001	4.36 ± 0.05	0.025 ± 0.001
Azo-AA : βCD-AA/Azo-AA = 1 : 40	7.71 ± 0.22	0.190 ± 0.002	3.94 ± 0.05	0.022 ± 0.001
μG-Azo1-Bis0	5.20 ± 0.23	0.081 ± 0.001	2.41 ± 0.04	0.011 ± 0.002

3 Complexation between Azo-AA and βCD-AA and stoichometry of the complex

3.1 Job's plot

In solutions, where two species are present (A and B), one A may bind to the other B. In some cases, more than one A will bind with a single B. A Job plot analysis is used to determine the amount of A binding to B. In this method, the sum of the molar concentrations of the two binding partners **Azo-AA** and **βCD-AA** is held constant, their mole fractions are varied (see Fig. S13). An observable that is proportional to complex formation is plotted against the mole fractions of these two components. For our case, as depicted in Fig. S13b we plotted a difference in absorbance ΔA versus the mole fraction. The results indicate a 1:1 binding stoichiometry.

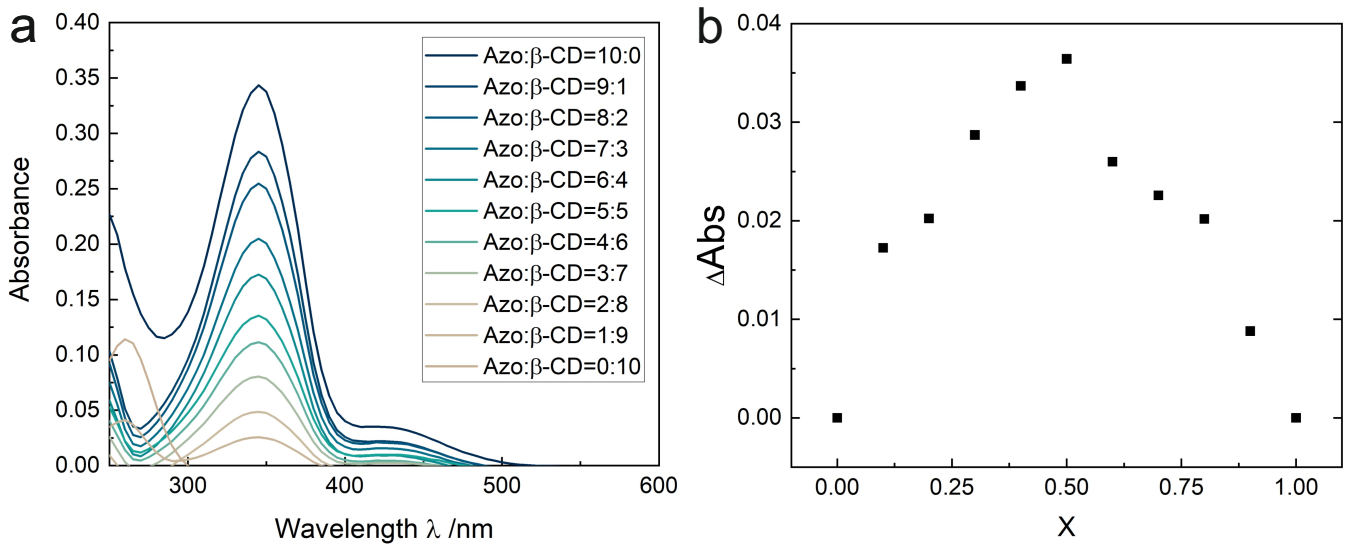

Figure S13 (a) Changes of UV-vis absorption spectra of **Azo-AA** and ***β*CD-AA** mixtures in water with [**Azo-AA**] + [***β*CD-AA**] $= 2.0 \times 10^{-5}$ mol/L. The concentration in 10^{-5} mol/L [**Azo-AA**] is varied from up to down: 2.0, 1.8, 1.6, 1.4, 1.2, 1.0, 0.8, 0.6, 0.4, 0.2, 0.

(b) Job's plot for the mixture with $\Delta A = \left|A - A_{\mathbf{Azo-AA}} \cdot x - A_{\boldsymbol{\beta}\mathbf{CD-AA}}(1-x)\right|$, where x indicates the mole fraction of **Azo-AA**, A the absorbance of the mixture and A_i the absorbance of 2.0×10^{-5} mol/L of pure compound i (**Azo-AA** or ***β*CD-AA**, respectively).

3.2 Association constants

The association constants K_a were determined by fitting the absorption data at a constant concentration of ***trans*Azo-AA** and ***cis*Azo-AA** with increasing ***β*CD-AA** concentrations applying the Benesi-Hildebrand equation:[3]

$$\frac{1}{A - A_0} = \frac{1}{A_{\max} - A_0} + \frac{1}{K_a \cdot (A_{\max} - A_0) \cdot [\boldsymbol{\beta}\mathbf{CD}]}$$

A_0 is the absorbance of the guest **Azo-AA** without ***β*CD-AA**, A is the absorbance with different concentrations of ***β*CD-AA**, $A_{\max}$ is the absorbance with the highest concentration of ***β*CD-AA**, and K_a is the association constant. For our system (1:1 complexes), K_a was determined from the slope m of $\frac{1}{A-A_0}$ versus $\frac{1}{[\boldsymbol{\beta}\mathbf{CD}]}$:

$$K_a = \frac{1}{m \cdot (A_{\max} - A_0)}$$

This way, the association constants were determined to be 1300 M^{-1} for ***trans*Azo-AA** and ***β*CD-AA**, and 20 M^{-1} for ***cis*Azo-AA** and ***β*CD-AA**, respectively.[3,4]

4 Properties of the photo-responsive microgels

4.1 NMR spectrum

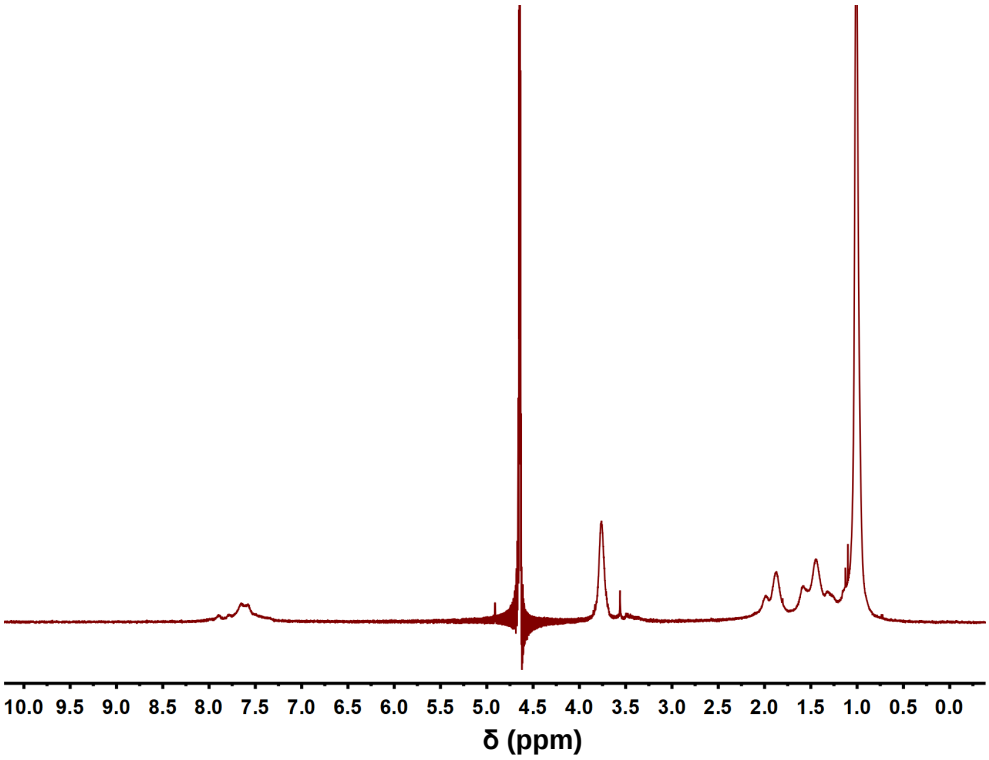

Figure S14 ^{1}H-NMR spectrum of **μG-Azo1-Bis2** (600 MHz, D_2O, 298 K)

4.2 FT-IR spectrum

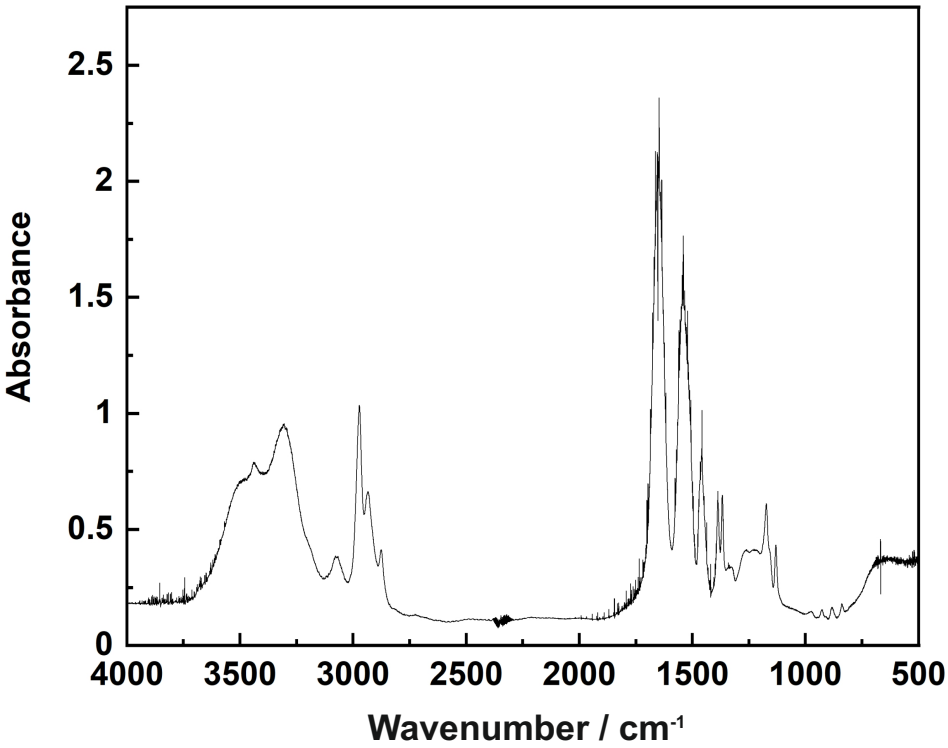

Figure S15 FT-IR spectrum of the **μG-Azo1-Bis2** microgels.

4.3 Reaction and incorporation amount of crosslinkers

Table S2 Added amounts of rectants and incorporated amount of **βCD-AA/Azo-AA** into the microgels **μG-Azo*x*-Bis*y***.

Microgel	NIPAM added	**βCD-AA/Azo-AA** added [mmol]	**βCD-AA/Azo-AA** added wt%	**βCD-AA/Azo-AA** incorp. wt%
μG-Azo1-Bis0	0.99	0.01	4.3	3.0
μG-Azo2-Bis0	0.98	0.02	7.9	4.6
μG-Azo1-Bis2	0.97	0.01	4.4	3.1
μG-Azo1-Bis4	0.95	0.01	4.4	3.4

4.4 Static light scattering

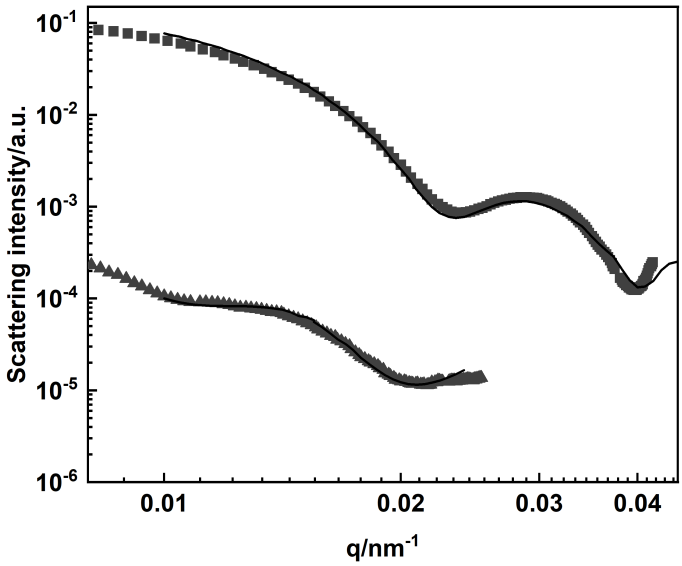

Figure S16 Form factors of **μG-Azo1-Bis2** (grey squares) and **μG-Azo1-Bis0** (grey triangle) probed by SLS at 20 °C. The data were fitted by a fuzzy sphere model[5] and the fits are presented as black solid line.

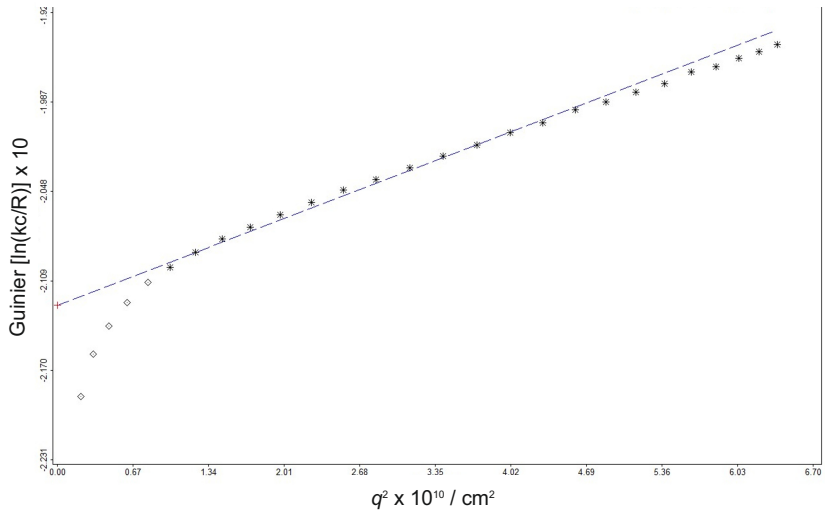

Figure S17 Guinier plot of static light scattering data of **μG-Azo1-Bis2**. The line presents a fit to the Guinier equation (see below).

A Guinier plot allows for the determination of the radius of gyration R_g from the measured scattered intensity as a function of the scattering vector q:

$$\ln\left(\Delta R(\theta)\right) = 1 - \frac{1}{3}R_g^2 q^2$$

Herein, ΔR is the excess scattering intensity, and the scattering wavevector at angle θ is $q = \frac{4\pi n_0}{\lambda}\sin\left(\frac{\theta}{2}\right)$, where λ is the wavelength of the laser and n_0 the refractive index of the medium.

Figure S17 shows a Guinier plot for a solution of **μG-Azo1-Bis2** in water at a concentration of 0.05 mg/mL, along with a fit to the Guinier approximation, which yields a radius of gyration R_g of 170 nm. The points measured at low angles are not included in the fit as these are likely affected by laser reflections.

4.5 Exemplary second order cumulant fit of dynamic light scattering data

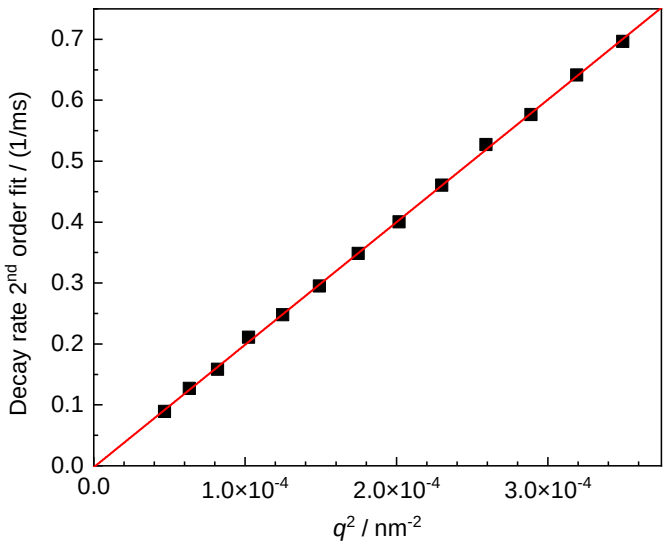

Figure S18 Example for a second order cumulant fit of dynamic light scattering data (see Experimental Part of the main paper).

5 Photo- and thermoresponsive behaviour

5.1 Temperature-dependent size changes in microgels with different crosslinkers

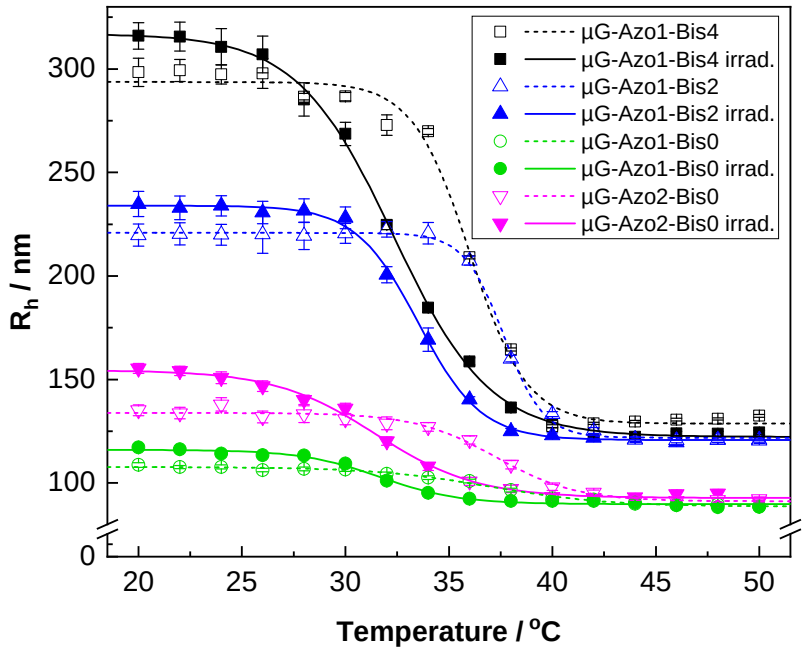

Figure S19 Temperature dependency of the hydrodynamic radii for the microgels (equivalent to Figure 3 of the main paper).

The temperature-dependent DLS curves for different microgels in water are shown in Fig. 3 of the main paper and in Figure S19. They were fitted with the following sigmoid function:

$$R_h(T) = \Delta R\left(1 - \frac{1}{1+\exp\left(-w(T-T_{\mathrm{VPTT}})\right)}\right) + R_{\mathrm{coll}}$$

The fit values are given in Tab. S3.

Table S3 Fit values for the temperature-dependency of the hydrodynamic radii of microgels before irradiation (dashed curves in Fig. S19).

Microgel	ΔR / nm	w / °C^{-1}	T_{VPTT} / °C	R_{coll} / nm
μG-Azo1-Bis4	165	0.73	36.0	122
μG-Azo1-Bis2	99	1.05	37.6	121
μG-Azo1-Bis0	43	0.51	37.3	93
μG-Azo2-Bis0	19	0.35	37.0	89

Table S4 Fit values for the temperature-dependency of the hydrodynamic radii of microgels after irradiation (solid curves in Fig. S19) and difference ΔT_{VPTT} of the volume phase transition temperatures after and before irradiation into the photostationary state.

Microgel	ΔR / nm	w / °C^{-1}	T_{VPTT} / °C	R_{coll} / nm	ΔT_{VPTT} °C
μG-Azo1-Bis4	195	0.43	32.3	122	3.7
μG-Azo1-Bis2	113	0.66	33.5	121	4.1
μG-Azo1-Bis0	62	0.41	31.5	93	5.8
μG-Azo2-Bis0	26	0.53	31.7	89	5.3

Table S5 Fit values for the temperature-dependency of the hydrodynamic radii of microgel **μG-Azo1-Bis2** after irradiation with different wavelengths until reaching the photostationary state.

Microgel	ΔR / nm	w / °C^{-1}	T_{VPTT} / °C	R_{coll} / nm	ΔT_{VPTT} °C
before irradiation	99	1.05	33.5	121	-
after irradiation with 365 nm	113	0.66	37.6	121	4.1
after irradiation with 400 nm	105	0.57	36.7	121	3.2
after irradiation with 425 nm	104	0.78	35.4	120	1.9

5.2 Viscosity

The viscosity of **μG-Azo1-Bis2** was measured by Capillary Viscometer (Cannon instruments).[6] The tube was immersed on a water bath held at T = 20 °C. The flow times were recorded using an automated detection system. The kinematic viscosity is calculated from these flow times using the K constant provided by the manufacturer. The specific viscosity of a dilute colloidal dispersion is related to the volume fraction ϕ of the pervaded volume of the colloids by $\eta_{sp} = 2.5 \times \phi$. The changes in the specific viscosities observed in Figure S20 for **μG-Azo1-Bis2** correspond to changes in microgel volume of approx. 16%, which are consistent with the behaviour observed by dynamic light scattering in Figure 5 of the main manuscript for this system.

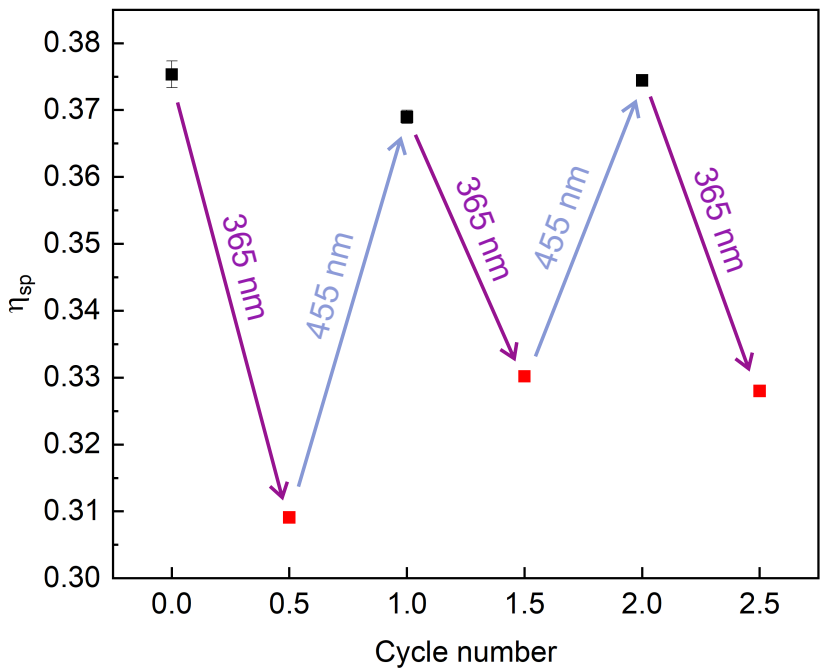

Figure S20 Reversible specific viscosity (η_{sp}) of **μG-Azo1-Bis2** with alternate light irradiation over several cycles (0.5 mg/mL in H_2O, 20 °C, λ_{UV} = 365 nm, 5.38 W m^{-2}; λ_{Vis} = 455 nm, 22.1 W m^{-2}). The black squares represent the original viscosity, the red squares represent viscosity after UV irradiation.

5.3 Spectra of photostationary state after irradiation of the μGs with different wavelengths

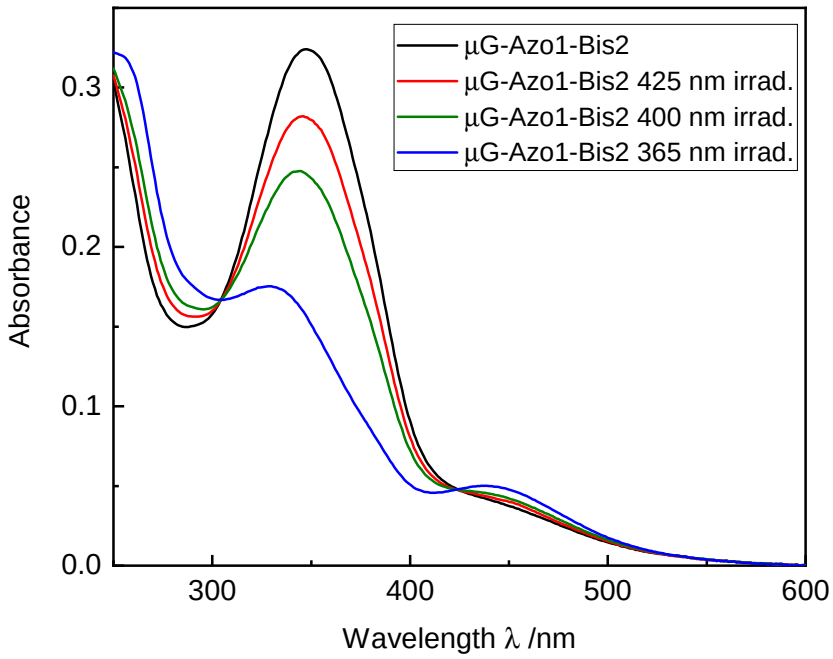

Figure S21 UV-Vis absorption spectra of photo-responsive microgels **μG-Azo1-Bis2**: (black) initial ***trans*Azo** form, (red) UV irradiation at 425 nm, (green) UV irradiation at 400 nm, (blue) UV irradiation at 365 nm.

5.4 Thermal back-switching from photostationary state to transAzo

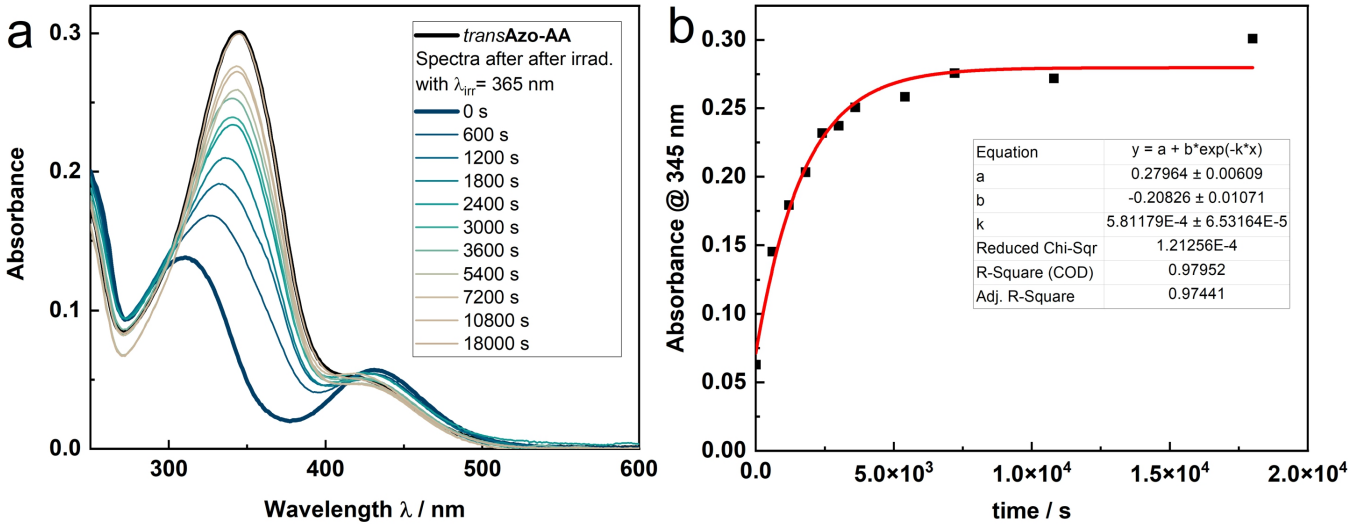

Figure S22 (a) Time series of spectra of ***trans*Azo-AA** in water: at 22 °C the solution was irradiated with 365 nm until the photostationary state was reached. Subsequently, keeping 22 °C, the thermal back-reaction was observed by UV-Vis spectroscopy. (b) Fitting of the kinetics at 345 nm with an exponential function yielding a rate constant of 5.81 $\times$ 10^{-4} s^{-1} corresponding to a lifetime of 29 min.

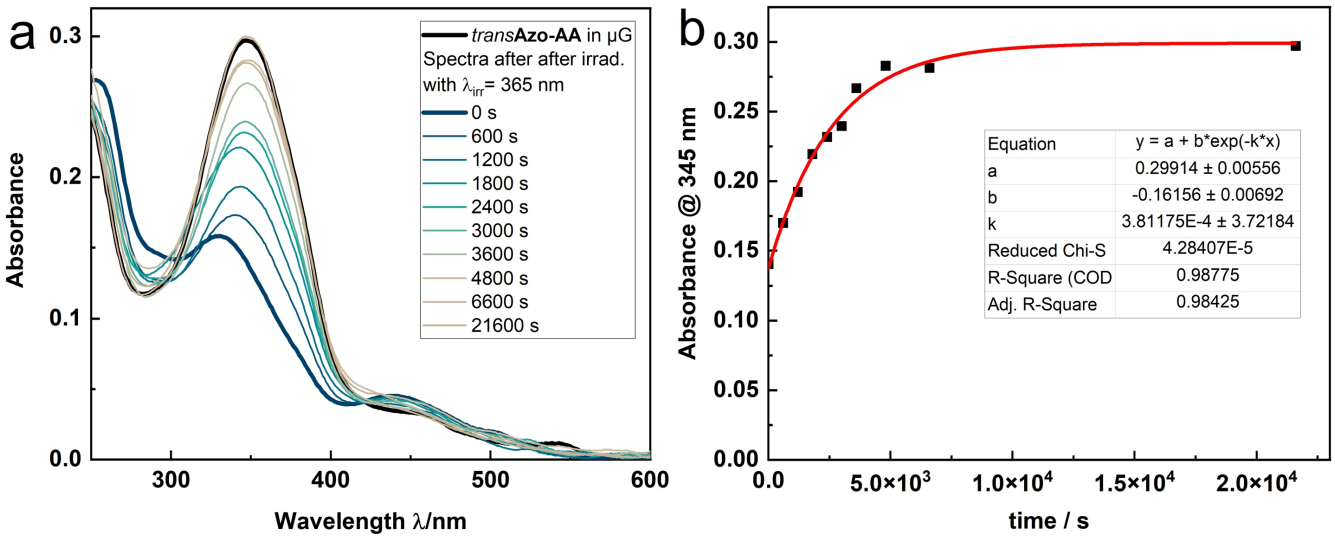

Figure S23 (a) Time series of spectra of microgels with **βCD-AA/Azo-AA** crosslinking in water: at 22 °C the solution was irradiated with 365 nm until the photostationary state was reached. Subsequently, keeping 22 °C, the thermal back-reaction was observed by UV-Vis spectroscopy. (b) Fitting of the kinetics at 345 nm with an exponential function yielding a rate constant of 3.81 $\times$ 10^{-4} s^{-1} corresponding to a lifetime of 44 min.

6 Size and morphologies investigated with TEM

The morphology of the photo responsive microgel **μG-Azo1-Bis0** was investigated with transmission electron microscope (TEM) as shown in Figure S24. The images illustrate that the microgels are of spherical shape and approx. 150 nm in diameter. The sizes from DLS of **μG-Azo1-Bis0** are slightly bigger than the sizes from TEM since the microgels in TEM are measured in the dry state. Besides, TEM measurements do not show a clear trend of expansion after irradiation, probably because of the limited expansion rate. However, after irradiation the dried microgels on the surface spread more and in an irregular way. This is an additional indication for the cleavage of crosslinks during irradiation.

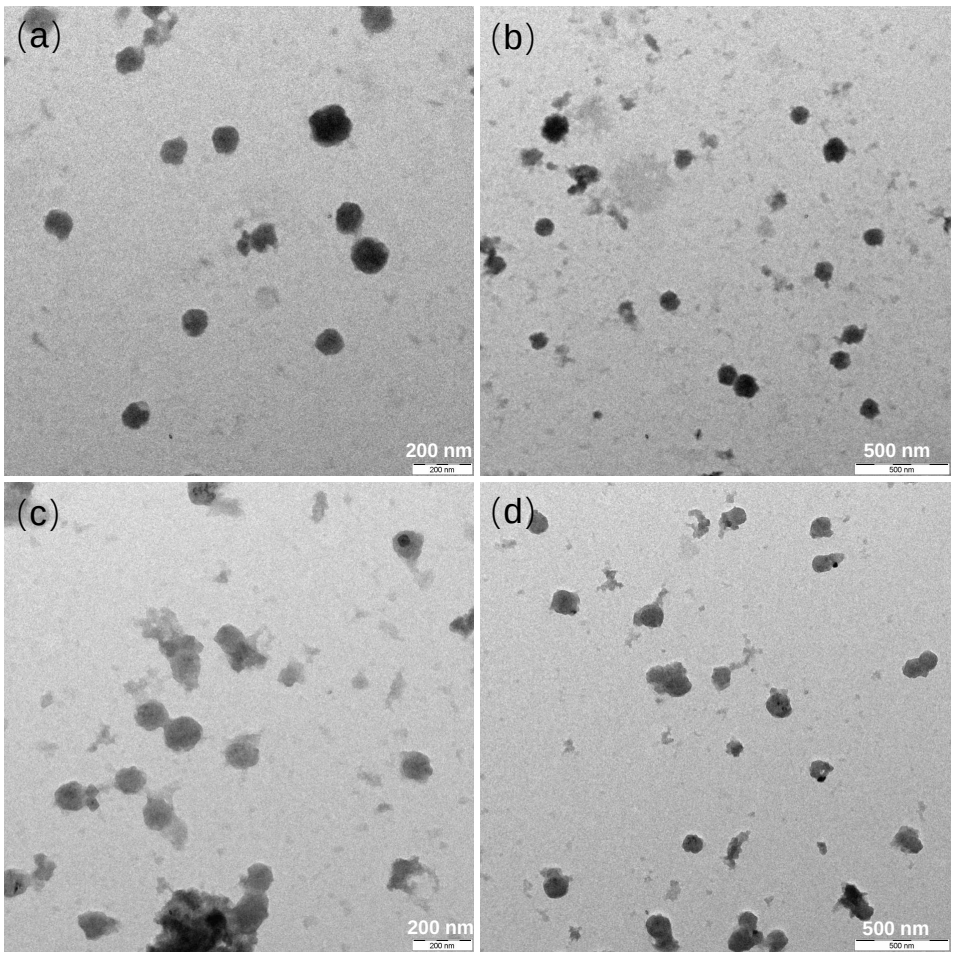

Figure S24 TEM images of **μG-Azo1-Bis0**: (a,b) before UV irradiation, (c,d) after UV irradiation for 15 min (0.2 mg/mL, λ_{UV} = 365 nm, 5.37 W m^{-2}).

Notes and references

1 W. Tang and S. C. Ng, *Nat. Protoc.*, 2008, **3**, 691–697.

2 A. Bouzide and G. Sauve, *Org. Lett.*, 2002, **4**, 2329–2332.

3 H. A. Benesi and J. H. Hildebrand, *J. Am. Chem. Soc.*, 1949, **71**, 2703–2707.

4 K. Srinivasan, T. Stalin and K. Sivakumar, *Spectrochim. Acta A Mol. Biomol.*, 2012, **94**, 89–100.

5 M. Stieger, W. Richtering, J. S. Pedersen and P. Lindner, *J. Chem. Phys.*, 2004, **120**, 6197–6206.

6 W. Richtering and H. Müller, *Langmuir*, 1995, **11**, 3699–3704.